PNAS RESEARCH ARTICLE | EARTH, ATMOSPHERIC, AND PLANETARY SCIENCES
EVOLUTION OPEN ACCESS

Endothermic physiology of extinct megatooth sharks

Michael L. Griffiths[a,1,2], Robert A. Eagle[b,c,1,2], Sora L. Kim[d,1,2], Randon J. Flores[b,c], Martin A. Becker[a], Harry M. Maisch IV[e], Robin B. Trayler[d], Rachel L. Chan[d], Jeremy McCormack[f], Alliya A. Akhtar[a,g], Aradhna K. Tripati[b,c], and Kenshu Shimada[h,i,j,2]

Edited by Thure Cerling, The University of Utah, Salt Lake City, UT; received October 24, 2022; accepted April 20, 2023

The evolution of the extinct megatooth shark, *Otodus megalodon*, and its close phylogenetic relatives remains enigmatic. A central question persists regarding the thermophysiological origins of these large predatory sharks through geologic time, including whether *O. megalodon* was ectothermic or endothermic (including regional endothermy), and whether its thermophysiology could help to explain the iconic shark's gigantism and eventual demise during the Pliocene. To address these uncertainties, we present unique geochemical evidence for thermoregulation in *O. megalodon* from both clumped isotope paleothermometry and phosphate oxygen isotopes. Our results show that *O. megalodon* had an overall warmer body temperature compared with its ambient environment and other coexisting shark species, providing quantitative and experimental support for recent biophysical modeling studies that suggest endothermy was one of the key drivers for gigantism in *O. megalodon* and other lamniform sharks. The gigantic body size with high metabolic costs of having high body temperatures may have contributed to the vulnerability of *Otodus* species to extinction when compared to other sympatric sharks that survived the Pliocene epoch.

regional endothermy | *Otodus megalodon* | clumped isotopes | fossil | extinction

Significance

Otodus megalodon was a gigantic shark that went extinct around 3.6 Mya. It could grow to the enormous size of at least 15 m long, making it one of the largest apex marine predators since the Mesozoic. Here, we test hypotheses relating to its extinction by providing quantitative estimates of its body temperature, thereby constraining its thermal physiology. We found that *O. megalodon* had body temperatures significantly elevated compared to other sharks, consistent with it having a degree of internal heat production as modern warm-blooded (endothermic) animals do. High metabolic costs associated with having at least partial endothermy may have contributed to its vulnerability to extinction compared to other shark species that persist until this day.

Sharks (Elasmobranchii: Selachii) are a group of cartilaginous fishes with a nearly 200-My geologic history (1). The fossil record shows that numerous shark taxa appeared and disappeared through geologic time where many clades even survived through the K-Pg mass extinction event (2–4). Today, there are over 500 species of sharks found in nearly every marine habitat, including the coastal epipelagic zone to below 1,000 m of depth in the abyssopelagic zone (5, 6). They play crucial roles in marine ecosystems as meso- and apex predators (7, 8) as well as potential food sources for older individuals or larger taxa (9).

As climate change warms oceans and estuaries worldwide, most certainly impacting the physiology of many fishes (10), one notable realization in recent decades has been the role of thermophysiological differences among marine vertebrates that plays on their geographic and bathymetric distributions (11, 12). For example, endothermic taxa can have higher cruising speeds that increase prey encounter rates as well as wider migration ranges compared to their ectothermic counterparts (13, 14). In fact, endothermy, the ability to metabolically elevate and retain body heat over a broad ambient temperature range (15), is regarded to have an evolutionary merit as demonstrated by the fact that it evolved multiple times in vertebrate history (16). In extant sharks, endothermy (more precisely, "regional endothermy") is confined to certain clades within the order Lamniformes, including *Alopias vulpinus* (Alopiidae: common thresher) as well as species of *Lamna*, *Isurus*, and *Carcharodon* (Lamnidae: mackerel sharks), typically induced by vascular countercurrent heat exchange and slow-twitch aerobic red muscles (13, 17, 18). Among lamnids, the average body temperature ranges from 22.0 to 26.6 °C and maximum reported body temperatures are elevated up to 10, 14, and 21 °C higher than ambient ocean temperature for *Isurus oxyrinchus* (shortfin mako), *Carcharodon carcharias* (white shark), and *Lamna ditropis* (salmon shark), respectively (ref. 19 and references therein).

The ability to regulate body temperature is evolutionarily profound because it is thought to have also acted as a key driver for the evolution of gigantism in macropredatory lamniform sharks (20). In fact, the iconic "megatooth shark," *Otodus megalodon* (Otodontidae) primarily known only from its gigantic teeth in the late Neogene fossil record suggesting it reached up to at least 15 m in length (21), is inferred to have been regionally endothermic based on multiple lines of evidence (22). As one of the largest carnivores to have ever existed on Earth, *O. megalodon* must have had a significant impact on the evolution of marine ecosystems (21). Thus, knowledge about the thermophysiology of *O. megalodon* and its effect on energetics, locomotion, foraging strategies, and distribution is critical to understand how its rise and demise influences the oceans' bioenergetics and trophic structures leading to today's marine conditions. Yet, the hypothesis that *O. megalodon* was

Author contributions: M.L.G., R.A.E., S.L.K., K.S., and M.A.B. designed research; M.L.G., R.A.E., S.L.K., R.J.F., R.B.T., R.L.C., and J.M. performed research; M.L.G., R.A.E., S.L.K., M.A.B., H.M.M., J.M., A.A.A., A.K.T., and K.S. contributed new reagents/analytic tools; M.L.G., R.A.E., S.L.K., R.J.F., R.B.T., and J.M. analyzed data; and M.L.G., R.A.E., S.L.K., R.J.F., R.B.T., and K.S. wrote the paper.

The authors declare no competing interest.

This article is a PNAS Direct Submission.

[1]M.L.G., R.A.E., and S.L.K. contributed equally to this work.

[2]To whom correspondence may be addressed. Email: griffithsm@wpunj.edu, robeagle@g.ucla.edu, skim380@ucmerced.edu, or kshimada@depaul.edu.

This article contains supporting information online at https://www.pnas.org/lookup/suppl/doi:10.1073/pnas.2218153120/-/DCSupplemental.

Published June 26, 2023.

likely endothermic rests on nonempirical inferences (22) and remains unconstrained through quantitative body temperature determinations.

Here, we quantitatively test the "*O. megalodon* endothermy hypothesis" ("endothermy" in the broad sense to include regional endothermy or mesothermy) by constraining the absolute body temperatures of this iconic species, as well as other common Late Neogene sharks (i.e., *Carcharias taurus, C. carcharias/hastalis,* and *I. oxyrinchus*), and drawing comparisons with extant marine vertebrates. We do so through measuring the abundance of multiply substituted isotopologs (i.e., "clumped" isotopes) in bioapatite-bound carbonate of their teeth along with phosphate oxygen isotope ($\delta^{18}O_p$) analyses. We interpreted the $\delta^{18}O_p$ values using a Bayesian approach that models body temperatures (and their uncertainties) based on the established relationship between seawater (SW) temperature and $\delta^{18}O$ values as well as the oxygen isotope composition of phosphatic tissues (23). Carbonate-clumped isotope thermometry involving the analysis of mass-47 CO_2 and reported in Δ_{47} (per mil, ‰) notation is an emerging geochemical technique based on the thermodynamic preference of ^{13}C and ^{18}O to form bonds, or "clump," in the carbonate mineral lattice. The basis for this heavier isotope clumping relies on the principles of quantum mechanical and statistical thermodynamics, which predict multiply substituted isotopologs of CO_2 and the carbonate ion to have lower free energies, and hence are more stable than isotopologs with one or no heavy isotope (24). This thermodynamic preference for clumped isotopologs in carbonate thus forms the basis for reconstructing mineralization temperatures independent of bulk oxygen isotope composition of the parent fluid (24–26). The application of this method has been effective in reconstructing vertebrate body temperatures of reptiles and birds from eggshell carbonate, as well as sharks from carbonates in the bioapatite of teeth (25, 27–29). The advantage of utilizing shark teeth is that they mineralize by secretion of biological hydroxyfluoroapatite (i.e., bioapatite) during amelogenesis and dentinogenesis (30), producing an enameloid structure that has a solubility several orders of magnitude lower than that of calcite and thus is less susceptible to diagenetic alteration during deposition and fossilization. It is worth noting though that this does not always extend to the carbonate ion substituting within the bioapatite lattice (31), calling for a need to assess the robust preservation of structural carbonate (*SI Appendix, Text*).

Studies utilizing carbonate-bound Δ_{47} to infer thermophysiology in fossil vertebrates have shown this method to be particularly useful when the temperatures in species of "unknown" thermophysiological origins are compared with co-occurring fossils of "known" metabolisms; the premise being that any deviation in body temperature from their ambient environment (inferred from ectothermic species), or that predicted from an assumed body mass, should reflect the abilities of the species to change its core body temperature above or below its natural environment (27–29). Other studies have used the difference in $\delta^{18}O_p$ between marine reptiles and sharks and coexisting ectothermic bony fish species as a proxy for endothermy (22, 32). Because the $\delta^{18}O_p$ values of marine vertebrates reflect both the body temperature and composition of body water that is in steady state with environmental (sea)water (33, 34), any deviation in $\delta^{18}O_p$ values between co-occurring ectothermic [proxy for sea surface temperatures (SSTs)] and presumed endothermic species should indicate the degree to which a species could elevate its body temperature, assuming that they resided in seawater of similar isotopic composition. Here, we apply these methods involving paired measurements of Δ_{47} and $\delta^{18}O_p$ values in coexisting marine fossil fish and mammal species to experimentally elucidate the thermophysiology of *O. megalodon*. By comparing *O. megalodon* body temperature estimates from both isotope proxies against those of contemporaneous ectothermic species, we show that *O. megalodon* had an elevated body temperature of approximately 7 °C relative to its environment. Importantly, we also show that *O. megalodon* was warmer than co-occurring (i.e., from the same sedimentary strata) regional endotherms, *C. carcharias* and *I. oxyrinchus*.

Results

Geologic and Environmental Setting of Fossils. Elasmobranch tooth samples of Miocene/Pliocene age from multiple sedimentary rock formations at the periphery of the North Pacific and North Atlantic Oceans were analyzed here (*SI Appendix, Text*). These sites are unique in that most contain co-occurring ear (tympanic) bones of known marine endotherms (e.g., cetaceans), providing a useful comparative benchmark in assessing body temperatures of contemporaneous fossil carcharhiniform and lamniform sharks. Paired Δ_{47} and $\delta^{18}O_p$ analyses were conducted on specimens from the Burdigalian (~20 to 16 million years old [Ma]) Pungo River Formation and the Zanclean (~5 to 4 Ma) Yorktown Formation in North Carolina, USA, and Langhian (~16 to 14 Ma) Iwadono Formation and Zanclean Na-arai Formation in Japan. In addition, we conducted a suite of $\delta^{18}O_p$ analyses on teeth from Langhian units in California (Sharktooth Hill Bonebed), USA, and compared them with recent results from Burdigalian units from Germany (Kalkofen and Baltringer Formation) and Malta (Globigerina Limestone, Gozo) (35) (*SI Appendix, Text*). SSTs for these Miocene- and Pliocene-aged shark teeth at each site were estimated from a recent 109-member ensemble of climate model simulations (HadCM3) (36), which show strong model–proxy agreement for the global ocean for the Phanerozoic (Dataset S1).

Fossil Elasmobranch and Mammal Body Temperatures from $\delta^{18}O_p$. We analyzed teeth from a suite of extant and fossil sharks, along with a selection of Cetacean inner ear bones, for phosphate oxygen isotope composition to compare with temperature estimates from Δ_{47} measurements. Across all localities, the $\delta^{18}O_p$ values ranged from 20.7 to 23.7‰ for ectotherms (mean $\delta^{18}O_p \pm 1\sigma = 22.5 \pm 0.7$‰, n = 28), 20.7 to 24.2‰ for regional endotherms (22.0 ± 0.9‰, n = 23), 20.3 to 21.8‰ for *Otodus* (21.3 ± 0.5‰, n = 16), and 18.5 to 21.0‰ for cetaceans (20.0 ± 0.8‰, n = 8) (Dataset S1). The $\delta^{18}O_p$ range for all taxa reflects the environmental variation (i.e., temperature, salinity, and $\delta^{18}O_{sw}$ changes) experienced by the individual during bioapatite mineralization. Shark teeth form relatively quickly and capture a geochemical snapshot with subsequent replacement teeth continuously forming (37). The variation within a locality could result from migratory behavior and movement of individuals between environments or seasonal oscillations as demonstrated by previous studies comparing isotope-enabled climate model outputs with fossil shark teeth (37, 38).

Following previous studies featuring $\delta^{18}O_p$ values, we calculated the $\delta^{18}O_p$ difference between coexisting *Otodus* species and ectothermic taxa across all sites, and then plotted this difference as a function of $\delta^{18}O_p$ values of ectothermic taxa (*SI Appendix*, Fig. S1). In addition, we plotted this relationship alongside previously published $\delta^{18}O_p$ values from teeth of taxa in the Cretaceous–Miocene megatooth shark (otodontid) lineage (ref. 22 and references therein). Following the methodology of Bernard et al. (32), calculated regression lines that have a more negative slope (i.e., those closer to −1) imply that body temperatures for the species in question are independent of ambient seawater temperatures. Calculated regression lines with and without our data

show no significant difference in slopes (P_{slope} = 0.8197), and collectively, exhibit a significant deviation from a slope of 0 (P_{slope} = 0.0010) that would imply the taxa were ectothermic.

In addition, we go further than previous work to estimate the body temperature of shark species and the oxygen isotope composition of seawater from the enameloid $\delta^{18}O_p$ using a Bayesian model. Briefly, Bayesian statistics attempt to estimate the most probable values of parameters—in our case, $\delta^{18}O_{sw}$ and temperature—based on data ($\delta^{18}O_p$) and prior information about SST (36). Given the large uncertainties in Cenozoic $\delta^{18}O_{sw}$, we used a plausible range of $\delta^{18}O_{sw}$ priors considering: 1) modern gridded seawater values (39); 2) where available, previous estimates from prior publications (e.g., ref. 40 for North Carolina specimens); and 3) reasonable body temperature ranges for endotherms and ectotherms for each locality. We used a similar procedure to model the body temperature of endothermic taxa. We used a vague uniform prior of between 10 to 45 °C (i.e., the full range of plausible body temperatures) (*SI Appendix*, Table S1). The advantage of this Bayesian modeling approach is the accurate and formal consideration of error when estimating temperature with prior information included in each series of modeling. The full details of our modeling, prior distributions, and posterior samples for each locality are available in supplemental information and at github.com/robintrayler/bayesian_phosphate. The ectothermic elasmobranchs in this study resulted in mean temperatures in Miocene California of 17.1 ± 1.4 °C, Miocene Germany of 21.2 ± 1.6 °C, Miocene Malta of 22.9 ± 2.1 °C, Pliocene Japan of 19.7 ± 4.1 °C, and Pliocene North Carolina of 19.4 ± 2.3 °C (*SI Appendix*, Table S2). The mean $\delta^{18}O_{sw}$ estimated from the ectothermic elasmobranchs was 1.4 ± 0.3‰ for California and 1.5 ± 0.3‰ for all other localities. The larger temperature variation for Pliocene Japan from the Bayesian model is likely due to the relatively low sample size.

Across all localities through the Miocene and Pliocene, temperature estimates indicate differences with thermal physiology. The Bayesian $\delta^{18}O_p$-based model estimated temperatures for *Otodus* of 27.0 ± 2.0 °C compared to known regional endotherms at 24.7 ± 1.5 °C and ectotherms at 21.3 ± 1.4 °C (Fig. 1 and *SI Appendix*, Table S2). One possibility that needs to be considered is that $\delta^{18}O_p$ differences among sympatric elasmobranchs, specifically the lower $\delta^{18}O_p$ values in *Otodus* taxa, could also reflect varying body water isotope values and/or ocean temperature habitats due to these elasmobranchs residing at different ocean depths and/or them having dissimilar seasonal migration patterns for hunting or reproduction. However, if *Otodus* species were capable of diving to great depths to forage, similar to modern *C. carcharias* (41), this behavior would lead to an increase in $\delta^{18}O_p$ values and therefore reduce the measured ^{18}O depletion relative to ectothermic species. Similarly, deeper waters would also result in higher bioapatite $\delta^{18}O_p$ values due to the much

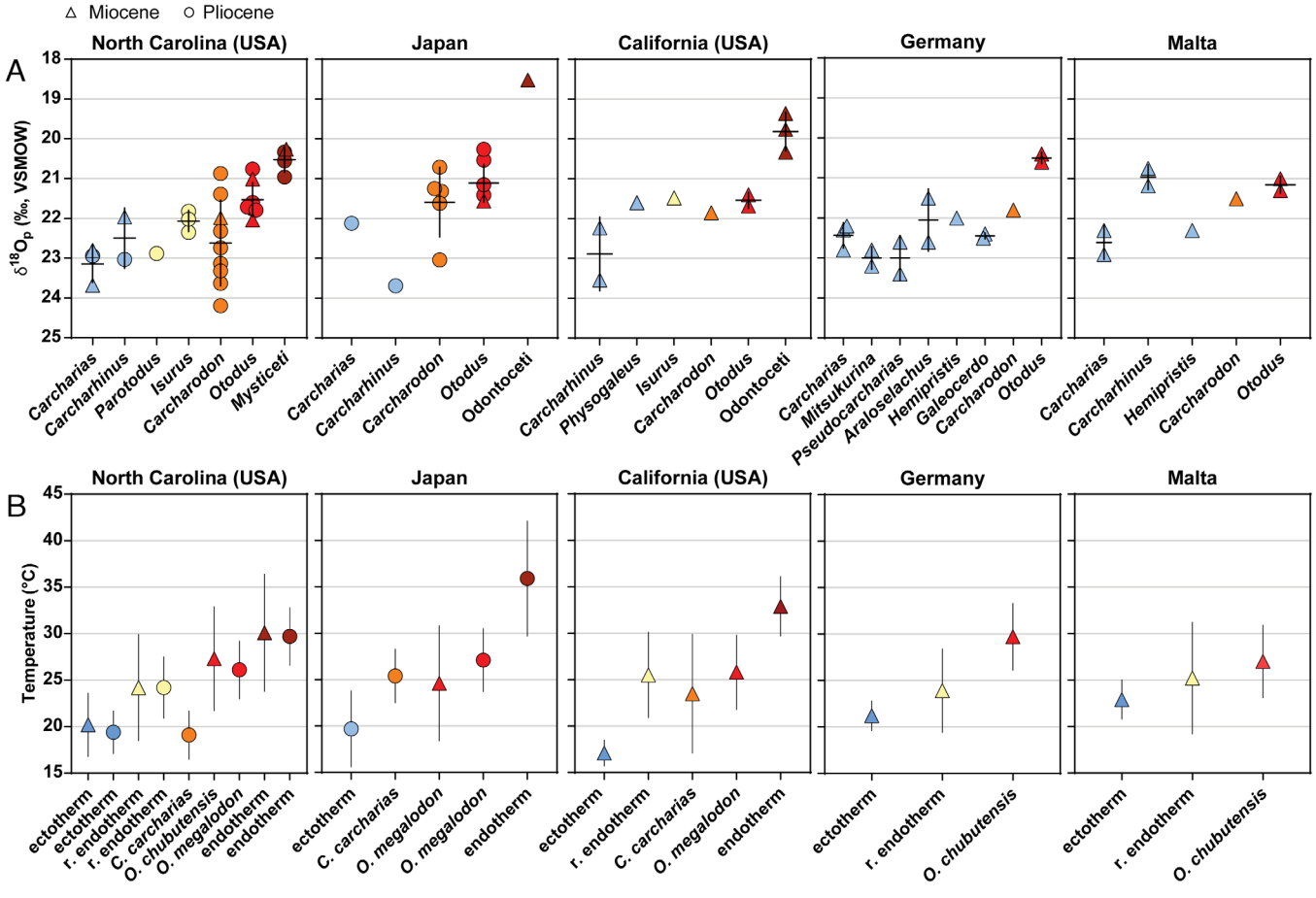

Fig. 1. Shark teeth from various Miocene (triangle) and Pliocene (circle) localities provide phosphate oxygen isotope compositions ($\delta^{18}O_p$) that reveal thermal physiology with temperature differences among sampled taxa. (*A*) The five localities provide context for *Otodus* (red) with comparisons to ectothermic (blue) sharks, predicted or known (yellow and orange based on extant *Isurus oxyrinchus* and *Carcharodon carcharias*, respectively) regionally endothermic (r. endothermic) sharks, and endothermic marine mammals (dark red). (*B*) Based on these $\delta^{18}O_p$ values, a Bayesian model correctly predicts body temperatures of endothermic marine mammals (dark red), distinguishes thermal differences among ectothermic (blue) and regionally endothermic (yellow and orange) sharks, and indicates elevated body temperatures in *Otodus* (red) similar to or beyond the extant *C. carcharias*. The Bayesian $\delta^{18}O_p$–based temperature model is described in the *Materials and Methods* section briefly with greater detail in *SI Appendix*, *Text*.

lower water temperatures with depth, which is again opposite to what we observe for *Otodus* relative to more surface-dwelling ectotherms. Another potential limitation relates to the differences in ocean temperatures between the Miocene and Pliocene for select locations, specifically the warmer Miocene SSTs that could be reflected in the ectothermic body temperature reconstructions. However, for those sites with both Miocene- and Pliocene-aged fossils (i.e., North Carolina and Japan), the derived body temperatures of species with similar thermophysiologies are almost identical across the two time periods (Fig. 1*B*). This is likely due to: 1) the small changes in mean SSTs (1–3 °C) between the Miocene and Pliocene at all sites (*SI Appendix*, Table S2); and/or 2) each species maintained consistent ocean habitats across geologic time. Adding weight to the latter, it was recently demonstrated from Zn and N isotopes that ectothermic piscivorous elasmobranchs from these same geologic units had a relatively constant trophic level across the Cenozoic (35, 42). Thus, the homogeneous population of $\delta^{18}O_p$ values (21.3 ± 1.4‰, n = 22) and consistent Bayesian-derived temperature offsets between *Otodus* and sympatric ectotherms (ΔT = 6.9 ± 1.6 °C; *SI Appendix*, Table S2) across the five distinct locations suggest that the elevated body temperature signal is robust.

The Δ_{47}–Temperature Relationships in Measurements on Modern Shark Tooth Bioapatite are Indistinguishable from Relationship in Carbonates. The prior knowledge of seawater temperature and $\delta^{18}O$ values remain key uncertainties in the application of oxygen isotope composition to discern body temperature of fossil organisms. Therefore, to alleviate these uncertainties, we also applied carbonate-clumped isotope thermometry to this question of megatooth shark body temperatures. Since the first measurements reported on vertebrate bioapatite (25), there have been relatively few clumped isotope measurements of marine vertebrates and none on the latest reference frame (43–46) based on a common carbonate standardization approach. Thus, to place our interpretations from fossil sharks on a strong footing and to provide up-to-date analyses of the relationships between Δ_{47} and bioapatite formation temperatures, we carried out analyses on teeth from 11 taxa including ectothermic sharks and bony fish as well as endothermic shark and mammal species (Fig. 2) (see *Materials and Methods* for further details on species measured). Formation temperatures span a temperature range of 7 to 36.7 °C and represent 52 Δ_{47} measurements conducted on 16 samples in total for an average of three replicate analyses per sample (Dataset S2).

A regression line following the method of York et al. (48) through our bioapatite data is described by the following equation:

$$\Delta_{47} = (0.0325 \pm 0.0093) \times 10^6 \times T^{-2} - (0.224 \pm 0.116), \quad [1]$$

where the uncertainty in slope and intercept is represented as the 95% confidence levels of the regression parameters. This regression overlaps with the 95% CI of the composite regression of Anderson et al. (47) described in Eq. **2**:

$$\Delta_{47} = (0.0391 \pm 0.0004) \times 10^6 \times T^{-2} - (0.157 \pm 0.004). \quad [2]$$

A hypothesis test performed to identify differences in slope and intercept of regressions where uncertainty in both x and y variables is present (see *Materials and Methods* for a description of regression comparisons) yields *P*-values of 0.537 and 0.775 for slope and intercept, respectively, indicating no significant differences between the lines.

This analysis supports the findings of Eagle et al. (25), which showed that the temperature relationships of carbonate-clumped isotopes in bioapatite and the inorganic calcite are indistinguishable, but now with an up-to-date data handling using current community and laboratory practices [the Intercarb-Carbon Dioxide Equilibrium Scale (I-CDES) reference frame] (43–46). Additional comparison of our calibrations to other published work can be found in *SI Appendix*. As the apatite calibration was statistically indistinguishable from the Anderson et al. (47) calibration, the Anderson et al. (47) calibration was used to calculate formation temperatures of fossil specimens given it has a lower uncertainty due to being underpinned by more analyses.

Elevated Body Temperature of *O. megalodon* Relative to Environment. We constrained the environmental conditions of coastal North Carolina, which has the richest fossil tooth assemblages used in this study. We measured the clumped isotope compositions on three scallop shells from the Pliocene Yorktown Formation, and one scallop shell from the Miocene Pungo River

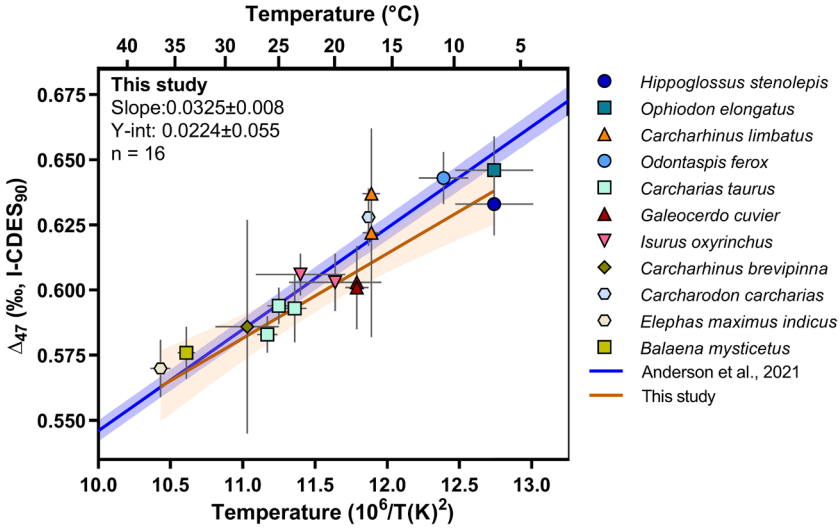

Fig. 2. Modern Δ_{47}-temperature calibration from wild-caught and aquarium-reared elasmobranch teeth, along with wild-caught bony fish and mammals. Lines indicate linear regressions calculated from our data (orange line and colored symbols) along with that of Anderson et al. (47) (blue line). Shaded regions surrounding regression lines indicate 95% CI. Error bars in the x and y directions on symbols indicate uncertainty in temperature and one external SE of the average Δ_{47}, respectively. Uncertainty in regression parameters indicates one SE.

Formation. Previous studies demonstrate that bivalves agree with the Δ_{47}–temperature relationships obtained for other recently published calibrations, allowing for robust reconstructions of seawater paleotemperatures (49–51). The Yorktown Formation scallops consist of material from single valves of *Chesapecten jeffersonius*, *Placopecten clintonius*, and *Carolinapecten eboreus*, whereas the Pungo River Formation is represented by an indeterminate species of *Chesapecten*. The Yorktown Formation scallops, *C. jeffersonius*, *P. clintonius*, and *C. eboreus,* yielded temperatures of 25, 21, and 18 °C, respectively, resulting in an average temperature of 21.3 ± 4 °C. This estimate is in general agreement (within uncertainty) with Pliocene temperature estimates from the region based on: 1) our Bayesian $\delta^{18}O_p$ body temperature estimates (19.4 ± 2.3 °C) from enameloid of ectothermic shark taxa collected from the Yorktown Formation (*SI Appendix*, Tables S1 and S2 and Dataset S1); 2) previously reported oxygen isotope compositions of molluscs from the same formation (40); and 3) climate model simulations (36). It is worth noting, however, that the derived $\delta^{18}O_{sw}$ values of the scallop species, *Chesapecten jeffersonius* and *Placopecten clintonius*, are ~2 ‰ higher than those previously reported for this location (40), while those of *Carolinapecten eboreus* are within the range of the previously estimated 1 to 2 ‰ seawater value. Thus, it is possible that the *C. jeffersonius* and *P. clintonius* shells had some degree of diagenetic alteration, producing slightly higher values than those reported from *C. eboreus* (*SI Appendix*, Fig. S3 and Dataset S2). On the contrary, the Δ_{47} temperatures for the dentine phase of *C. carcharias* and *O. megalodon* teeth from the Yorktown Formation, assumed to represent a diagenetic end-member, average 31 ± 7 °C (n = 9), significantly higher than those reported for the scallop shells. These observed tooth dentine and carbonate shell Δ_{47} temperature offsets suggest little or no geochemical alteration of the scallop species.

The enameloid of the Pliocene *O. megalodon* teeth from North Carolina yielded an average Δ_{47}-derived temperature of 26 ± 1 °C (n = 15). This is warmer than sympatric regional endotherms, *C. carcharias* (Δ_{47}: 20 ± 4 °C, n = 5) from North Carolina and *C. hastalis* (20 ± 3 °C, n = 5) from South Carolina (*SI Appendix, Text*), along with extant *C. carcharias* (18 ± 0 °C; Fig. 3 and Dataset S2). These temperatures also agree well with the Bayesian $\delta^{18}O_p$-based posterior mean temperature for North Carolina *O. megalodon* for the Pliocene (26.1 ± 3.1 °C), again exhibiting higher temperatures than those of *C. carcharias* (19.1 ± 2.6 °C) and all other non-*C. carcharias* regional endotherms (24.2 ± 3.3 °C) (Fig. 3 and *SI Appendix*, Table S2). The derived *O. megalodon* temperatures exceed the modeled annual SST estimate for the coastal Carolinas (~18 °C) (36) and are significantly warmer than those of the Δ_{47}-derived temperatures from the scallop shells (Welch's *t test*: $t = 2.16$, $P = 0.0398$). However, it is worth pointing out that the fossil shells likely have a warm season bias given the highly seasonal growth temperatures of these mid-latitude scallops (40). As such, our results may be underestimating the magnitude of *O. megalodon* tooth-derived temperature estimates. Moreover, comparison of Δ_{47} temperatures between shark tooth dentine and enameloid in Pliocene taxa reveals that isotopic resetting due to diagenesis in the Yorktown Formation is likely to result in higher Δ_{47}-derived temperatures. Therefore, considering any potential recrystallization of the carbonate shells, the 4–6 °C elevated body temperature of *O. megalodon* is likely at the lower end of estimation.

The Δ_{47}-derived body temperatures for *O. megalodon* teeth from Japan also yield temperatures (28 ± 4 °C, n = 14) that are warmer than those reported for sympatric *C. carcharias* (26 ± 0 °C, n = 5). The Bayesian $\delta^{18}O_p$-based model resulted in similar body temperatures in the Pliocene from Japan with *O. megalodon* mean temperatures of 27 ± 3 °C and 25 ± 3 °C for *C. carcharias*. The average derived temperature of *O. megalodon* is consistent with that of the North Carolina samples and maintains the relationship of elevated temperature with respect to the regionally endothermic *C. carcharias.* The derived temperatures of *O. megalodon* and *C. carcharias* from Japan are also both warmer than modeled annual SST estimates (~18 °C) (36). Without the additional constraint of Δ_{47}-derived seawater temperatures from invertebrates analogous to those sampled at the North Carolina site, it is challenging to confidently determine the offset in temperature from ambient water conditions exhibited by the specimens collected from Japan. However, consistently warmer temperatures observed in *O. megalodon* relative to *C. carcharias,* combined with consistent average body temperatures across all sites which exceed ectothermic species (proxy for SSTs) (Table 1) and modeled SST estimates, support the argument that *O. megalodon* had an elevated body temperature above the surrounding seawater temperature.

Discussion

Across all sites, the body temperatures of *Otodus* species average ~7 °C higher (ΔT) relative to ambient seawater temperatures as inferred from $\delta^{18}O_p$-offsets with sympatric ectothermic species (Figs. 1 and 3, Table 1, Dataset S1, and *SI Appendix*, Table S2). These elevated

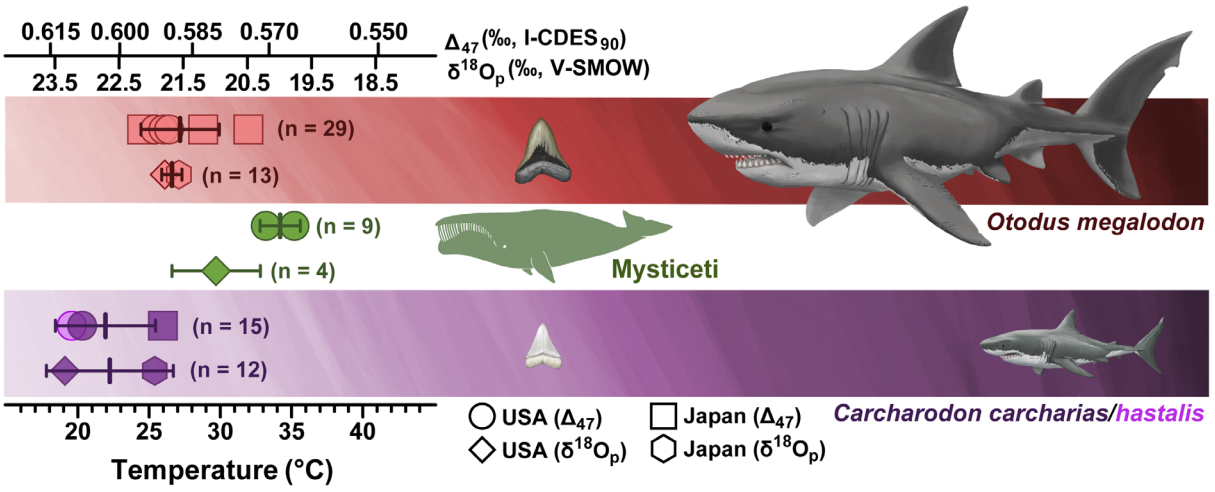

Fig. 3. Body temperature reconstructions of *O. megalodon,* Mysticeti, and the *Carcharodon* lineage (*C. hastalis* and *C. carcharias*) from the eastern United States (North Carolina) and Japan from Δ_{47} (n = 53) and $\delta^{18}O_p$ (n = 39) for the Pliocene. Shark illustrations by Christina Spence Morgan, copyright 2021.

Table 1. Δ_{47} and $\delta^{18}O_p$ measurements of specimens averaged across all locations and time periods

Thermoregulation or specific taxa	Δ_{47} ‰, I-CDES	# *n* analyses*	Δ_{47} Temp. (°C)†	$\delta^{18}O_p$ ‰, V-SMOW‡	# *n* analyses	$\delta^{18}O_p$ Temp. (°C)‡
Ectotherms§				22.1 ± 0.7	28	21.3 ± 1.4
Carcharodon	0.604 ± 0.008	15	22 ± 3	22.3 ± 0.8	13	22.7 ± 4.0
Otodus	0.588 ± 0.008	29	27 ± 3	21.2 ± 0.5	22	26.9 ± 4.2
Endotherms¶	0.569 ± 0.009	9	34 ± 3	20.3 ± 0.3	9	32.1 ± 5.0

The raw Δ_{47} data can be found in Dataset S2, while the raw data used to calculate the Bayesian-derived $\delta^{18}O_p$ temperatures can be found in Dataset S1.
*Represents the number of distinct CO_2 extractions from each sample that was separately purified and analyzed. Data for individual extractions are shown in Dataset S2.
†Calculated using the inorganic calibration of Anderson et al. (47) (Eq. **2**).
‡Estimated using a Bayesian modeling approach. See *SI Appendix, Text* for further details of the method. Model priors and posteriors are shown in Dataset S1 and *SI Appendix*, Tables S1 and S2.
§Represents the following species: *Mitsukurina lineata*, *Pseudocarcharias rigida*, *Araloselachus cuspidatus*, *Carcharias acutissimus*, *C. taurus*, *Carcharias* sp., *Parotodus benedini*, *Physogaleus* sp., *Hemipristis serra*, *Galeocerdo aduncus*, and *Carcharinus* sp.
¶Represents the following genera: Mysticeti and Odontoceti.

temperatures are also observed for sympatric regional endotherms, including *Isurus* (ΔT = 4 °C) and *Carcharodon* (ΔT = 3–8 °C), but are lower than those for endothermic whales, Odontoceti (ΔT = 10–14 °C) and Mysticeti (ΔT = 9–12 °C). These interpretations are also reproduced through an independent determination of ΔT values derived from the Δ_{47} temperatures (Fig. 3 and Table 1).

Notwithstanding these results, there are some notable limitations to interpreting our data as a diagnostic for endothermy in *Otodus* taxa. Indeed, one obvious shortcoming relates to the isotope-inferred body temperature reconstructions from the fossil teeth, which may underestimate the shark internal core temperatures due to conductive heat loss gradients from the innermost body temperatures (19). For example, estimates of extant *C. carcharodon* body temperatures from our clumped isotope measurements average 18 ± 0 °C (Fig. 3), while stomach temperatures are shown to be upward of 23 to 27 °C (52); this difference is due to the conductive heat loss gradient with cooler environmental water temperatures. Given that teeth are the only well-preserved substrate for geochemical analysis of sharks, extracting shark internal core temperatures from fossil remains will always be a challenge, but Δ_{47}-derived body temperature nevertheless provides at least a minimum estimate. In addition, there is some research which suggests cranial endothermy in salmon sharks, raising the possibility of heat generation in the jaws as well as direct transport of interior body heat to the cranium (53).

Another challenge relates to the exact body form of *O. megalodon*, which remains uncertain based on the present fossil record (54). An attempt to reconstruct body form using a 3D computer model rendering was made recently (55); however, its accuracy remains questionable given that the model requires many assumptions such as the cranial skeleton of *O. megalodon*, which is currently not known from the fossil record and no published record of teeth–vertebrae-associated specimens exist. Nevertheless, one of the rationales for using extant *C. carcharias* as a model organism in that study (55) was the assumption that *O. megalodon* was likely regionally endothermic (22). Although our isotope-based inference does not allow a decisive determination of whether *O. megalodon* was "wholly" or only "regionally" endothermic, it is reasonable to assert that it was indeed a regional endotherm given that its inferred body temperature range in our study is warmer than that of ectotherms and colder than that of true endotherms (marine mammals) that lived contemporaneously. Therefore, our study has offered empirical support for the "*O. megalodon* endothermy hypothesis".

If the results of the recent 3D body form reconstruction are considered at face value, *O. megalodon* measuring lengths of up to 20 m would have weighed about 61.5 t (55). If so, the elevated and stable body temperatures of *Otodus* across all locations could, at least in part, be attributed to "gigantothermy"—i.e., the link between low surface area-to-volume ratios scaled to heat retention in animals. Indeed, field experiments on the modern shark equivalent to *O. megalodon* [in terms of its estimated maximum body length of 15 to 20 m: (21, 56)], the whale shark (*Rhincodon typus*), have recorded a stable internal body temperature of around 27 °C despite being an ectotherm (57). Interestingly, temperature-tracking data also show that whale sharks maintain a relatively high body temperature even when diving to great depths (>1,300m) for extended periods (12+ hours). This "inertial homeothermy" associated with massive size may have also operated in the size-equivalent *O. megalodon*, implying that its relative thermal stability across different ocean basins and environments could be linked to this phenomenon. On the contrary, *O. megalodon* and its immediate chronospecies predecessor, *O. chubutensis*, were apex predators feeding at a high trophic level in contrast to filter-feeding whale sharks (35, 42). Hence, a regionally endothermic physiology of *Otodus* deciphered from temperature estimates based on our Δ_{47} and $\delta^{18}O_p$ values is compatible with their trophic level and inferred predatory lifestyle, which would have required a high metabolic rate.

Our evidence for *O. megalodon* regional endothermy has significant implications to the ecology and evolution of this prehistoric shark as well as its possible extinction mechanism(s). Although elucidation of its exact body mass and morphology requires improvement in the available fossil record of *O. megalodon* skeletal remains (54), the confirmation of its endothermic physiology in the fossil species is one step forward in understanding its paleobiology. For instance, endothermic fishes are said to have evolved to increase their swimming speed (14), allowing them to move greater distances and thereby increasing their prey encounter rates (13). Furthermore, regional endothermy formed a critical evolutionary pathway to gigantism in *Otodus* (20), which likely promoted its true competitive superiority, coupled with an increased tolerance to cooler waters (58).

Our study also contributes to the much-debated possible causation of *O. megalodon* extinction. Some studies have invoked changes in the diversity, size, and abundance of baleen whales (mysticetes) due to a reduction in productive coastal habitats during the Pliocene as a cause for the demise of *O. megalodon* (59, 60). Recent investigations utilizing N and Zn isotopes to infer trophic-level changes in megatooth sharks suggest that *O. megalodon* was a significant apex predator, residing at the top of the marine food chain (35, 42). In addition, these chemical proxies for trophic level indicate variation in *O. megalodon* diet, perhaps a response to the emergence of likely competitors (e.g., *C. carcharias*) and/or new prey species (e.g., smaller baleen whales) (35). As a gigantic apex predator, *O. megalodon* would have incurred high metabolic costs imposed by its regionally endothermic physiology and coupled with its top trophic-level diet, as suggested by previous studies, there were likely high bioenergetic demands (61). This precarious energetic balance was perhaps put in peril when productive coastal shelf habitats diminished and there were accompanying shifts in prey landscapes

due to Pliocene sea-level changes. Indeed, prior work has shown regional endothermy to be associated with high extinction risk among large-bodied species, especially when large prey become scarce (60). Therefore, our results contribute to the growing body of work demonstrating that despite having traits that allowed them to be a commanding presence in the ocean, marine apex predators such as *O. megalodon* were not immune to the effects of climate change, highlighting the need for conservation efforts to protect modern shark species, including the great white shark.

Materials and Methods

Modern Samples and Body Temperature Estimates. All shark tooth samples used in this study were collected legally and ethically. All fossil samples and majority of extant samples were housed in the following four repository institutions (Datasets S1 and S2): Calvert Marine Museum (CMM), Solomons, MD, USA; San Diego Natural History Museum (SDNHM), San Diego, California, USA; Bernice P. Bishop Museum (BPBM), Honolulu, USA; and Los Angeles County Museum, Los Angeles, California, USA. The following individuals aided in securing or loaning the reposited samples for destructive analysis: D. Ward, M. A. Becker, I. Samson, J. Wheeley, G. Cliff, T. Deméré, S. Godfrey, H. M. Maisch IV, J. Nance, K. Shimada, A. Suzumoto, B. Welton, P. Sternes, Koji Fujii, Yukito Kurihara, Akihiko Sekita, Sho Tanaka, and Tomoyasu Yamamoto. A detailed description of the geological setting associated with each of the fossil samples is provided in *SI Appendix*.

Formation temperature estimates of wild-caught sharks and bony fish were derived from in situ measurements of water temperature at the time of capture or estimated from observations (using HadISST) based on the date of capture. In the case of the smalltooth sand tiger shark (*Odontaspis ferox*) samples from Hawaii, caught on April 1969 in a gill net from a depth of ~275 m (62), temperature estimates were averaged from measurements taken from a submarine (September 1968) and a bathythermograph (April 1969). For samples where no reliable water temperature measurements were readily available, temperature estimates were derived from $\delta^{18}O_p$ values performed on subsets of the same specimens used here (63), employing the empirical equation of Kolodny et al. (23) and assuming a local seawater $\delta^{18}O$ ($\delta^{18}O_{sw}$) value of 0.5‰ measured at the time of capture (63). Aquarium-reared samples were collected from the London Aquarium, Birmingham Aquarium, and Tokyo Sumida Aquarium where water temperatures were held stable at 25, 23.6, and 26 °C, respectively. The endothermic taxa included in the calibration consisted of tooth enamel from an Indian elephant (*Elephas maximus indicus*) and highly mineralized (64) ear bone material from a bowhead whale (*Balaena mysticetus*). Indian elephants have been shown to have body temperatures ranging from 35.9 to 36.7 °C (65), while the bowhead whale maintains a body temperature of approximately 33.8 °C (66).

Clumped Isotope (Δ_{47}) Analysis. All teeth were cleaned by ultrasonication in ultrapure water (Milli-Q water) for 15 min prior to destructive sampling. Modern and fossil shark tooth enameloid and dentine powders (~300 to 500 mg) were abraded using a Dremel drill equipped with a 300-µm diamond–tipped bit and operated at slow speed at William Paterson University (Wayne, NJ). Following the protocol of Eagle et al. (27), bioapatite samples were soaked in hydrogen peroxide for 4 h, soaked in 0.1M acetic acid, buffered to pH 4.6 in 1M sodium acetate for 14 h, and then rinsed three times with Milli-Q water prior to isotopic analysis.

Clumped isotope analyses were conducted in the Eagle-Tripati lab at the University of California, Los Angeles, between 2015 and 2022. Samples were analyzed on two Nu Perspective IS mass spectrometers which have been demonstrated to produce statistically indistinguishable results for Δ_{47} (46). Both instruments prepared samples for analysis through digestion in a common acid bath containing 105 wt% phosphoric acid reacted at 90 °C followed by multiple steps of cryogenic purification and passage through a GC column packed with Porapak Type-QTM 50/80. Following purification, sample CO_2 gas was then introduced into the IRMS system via an automated changeover block, allowing for continuous alternating measurements of sample and reference CO_2 gas on detectors configured to measure isotopologs of masses 44, 45, 46, 47, 48, and 49. Measurements taken in bellows mode (~100 to 300 mg of sample material) consisted of four blocks of 20 cycles totaling in 1,600 s of integration with balancing to maintain 80 nA on mass 44 at every acquisition, while samples conducted in microvolume mode (30 to 100 mg of sample material) consisted of three blocks of 20 cycles for a total of 1,200 s of integration and a range of 80 nA to 30 nA over the course of each acquisition.

Carbonate standards ETH-1 and ETH-2 were used to perform a nonlinearity correction on sample unknowns. These nonlinearity-corrected values were then projected into the I-CDES reference frame of Bernasconi et al. (43) using ETH-1,2, and 3 along with three in-house standards. ETH-4 was not included in the corrections and was instead used as a check for data quality. Corrections were applied to sample and standard data over a moving average of 10 standards on either side of a given sample and were calculated using the Easotope software package (67).

Phosphate Oxygen Isotope ($\delta^{18}O_p$) Analysis. Enameloid samples were powdered with a slow-speed Dremel dental drill equipped with a 300-µm diamond–tipped bit, then silver phosphate was precipitated following Mine et al. (68). Further details on the protocol can be found in *SI Appendix, Text*.

Statistical Analyses of Clumped Isotope and Phosphate $\delta^{18}O$ Data. We used the equation of Kolodny et al. (23) recast into a Bayesian framework to estimate the temperature and oxygen isotope composition of seawater from our enameloid $\delta^{18}O_p$ values. This relies on the established relationship among temperature, $\delta^{18}O_{sw}$, and the oxygen isotope composition ($\delta^{18}O_p$) of phosphatic tissues in a variety of organisms including several species of fish (62) and sharks (63, 69). In particular, the Bayesian approach allows us to estimate the uncertainties in body temperature associated with changes in seawater temperature and oxygen isotope composition. Briefly, we assume that $\delta^{18}O_p$ is proportional to a normal distribution [$\delta^{18}O_p \sim N(\mu, \sigma)$] where μ is the phosphate-temperature equation of Kolodny et al. (23) and σ is a dispersion term estimated from the data. This formulation allows for robust estimations of uncertainty for both temperature and $\delta^{18}O_{sw}$ and allows the incorporation of prior information of the credible range for these parameters. The full details of our model and implementation are available in *SI Appendix*, Text 2.3.

Linear regressions were performed using the york function of the IsoplotR package for RStudio. Hypothesis testing to compare regression slopes and intercepts was conducted using the sma function of the SMATR package for RStudio in order to compare regressions through separate datasets with errors in both the x and y directions.

Data, Materials, and Software Availability. Clumped isotope data have been deposited in EarthChem (https://doi.org/10.26022/IEDA/112933) (70). Previously published data were used for this work [A portion of the phosphate oxygen isotope data (i.e., the Germany and Malta data in Fig. 1) was recently reported in supplementary figure 8 in ref. 35 (https://www.nature.com/articles/s41467-022-30528-9)].

ACKNOWLEDGMENTS. This research was supported by a NSF Sedimentary Geology and Paleobiology Award to M.L.G. and M.A.B. (Award #1830581), R.A.E. (Award #1830638), K.S. (Award #1830858), and S.L.K. (Award #1830480), and an American Chemical Society Award, Petroleum Research Fund Undergraduate New Investigator Grant PRF #54852-UNI2 to M.L.G. Randon Flores was supported by an early career fellowship from the Center for Diverse Leadership in Science funded by the Packard Foundation, Dahlio Philanthropies, Oceankind, the Sloan Foundation, and NSF. Clumped isotope mass spectrometry at UCLA was supported by DOE BES grant DE-FG02-83613ER16402 and Heising-Simons Foundation grant 2022-3314 to Aradhna Tripati. J.M. was supported by the Deutsche Forschungsgemeinschaft (DFG, German Research Foundation) project #505905610. We acknowledge the significant contribution from numerous undergraduate students from William Paterson University (Adanny Camacho, Chelesia Clarke, Tara Ekiert, Chris Gocklin, Bryan Gonzalez, Kyle Hansen, Allison Neumann, Drew Pedersen, Richard Plattel, and Fatima Popcakova), who helped to drill the powders from modern and fossil shark tooth samples used in this study as well as students from University of California, Merced, who prepared samples and helped generate the silver phosphate results (Gabriele Larocca Conte, Leslie Lopez Ostorga, Maya Morris, and Pedro Valencia Landa). We greatly acknowledge the help and support of the following individuals who aided in securing or loaning the reposited samples for destructive analysis: G. Cliff (Kwazulu-Natal Sharks Board), I. Sansom (University of Birmingham), J. Wheeley (University of Birmingham), T. Deméré (SDNHM), S. Godfrey (CMM), J. Nance (CMM), A. Suzumoto (BPBM), D. DeNardo (New York Aquarium), B. Welton, and P. Sternes. We thank Emma Kast for fruitful discussions on earlier versions of this manuscript.

Author affiliations: [a]Department of Environmental Science, William Paterson University of New Jersey, Wayne, NJ 07470; [b]Department of Atmospheric and Oceanic Sciences, Center for Diverse Leadership in Science, Institute of the Environment and Sustainability, University of California–Los Angeles, Los Angeles, CA 90095; [c]Department of Earth, Planetary, and Space Sciences, Center for Diverse Leadership in Science, Institute of the Environment and Sustainability, University of California–Los Angeles, Los Angeles, CA 90095; [d]Department of Life and Environmental Sciences, University of California–Merced, Merced, CA 95343; [e]Department of Marine and Earth Sciences, Florida Gulf Coast University, Fort Myers, FL 33965; [f]Institute of Geosciences, Goethe University Frankfurt, Frankfurt am Main 60438, Germany; [g]Department of Geosciences, Princeton University, Princeton, NJ 08544; [h]Department of Environmental Science and Studies, DePaul University, Chicago, IL 60614; [i]Department of Biological Sciences, DePaul University, Chicago, IL 60614; and [j]Sternberg Museum of Natural History, Fort Hays State University, Hays, KS 67601

1. J. Maisey, What is an "elasmobranch"? The impact of palaeontology in understanding elasmobranch phylogeny and evolution *J. Fish Biol.* **80**, 918–951 (2012).
2. J. Kriwet, M. J. Benton, Neoselachian (chondrichthyes, elasmobranchii) diversity across the cretaceous–tertiary boundary. *Palaeogeogr. Palaeoclimatol. Palaeoecol.* **214**, 181–194 (2004).
3. C. J. Underwood, Diversification of the neoselachii (Chondrichthyes) during the Jurassic and Cretaceous. *Paleobiology* **32**, 215–235 (2006).
4. R. A. Belben, C. J. Underwood, Z. Johanson, R. J. Twitchett, Ecological impact of the end-Cretaceous extinction on lamniform sharks. *PLoS One* **12**, e0178294 (2017).
5. R. A. Martin, Conservation of freshwater and euryhaline elasmobranchs: A review. *J. Mar. Biol. Assoc. U. K.* **85**, 1049–1074 (2005).
6. S. Weigmann, Annotated checklist of the living sharks, batoids and chimaeras (Chondrichthyes) of the world, with a focus on biogeographical diversity. *J. Fish Biol.* **88**, 837–1037 (2016).
7. R. A. Myers, J. K. Baum, T. D. Shepherd, S. P. Powers, C. H. Peterson, Cascading effects of the loss of apex predatory sharks from a coastal ocean. *Science* **315**, 1846–1850 (2007).
8. C. L. Lawson *et al.*, Powering ocean giants: The energetics of shark and ray megafauna. *Trends Ecol. Evol.* **34**, 1009–1021 (2019).
9. A. F. Navia, P. A. Mejía-Falla, J. López-García, A. Giraldo, V. H. Cruz-Escalona, How many trophic roles can elasmobranchs play in a marine tropical network? *Mar. Freshwater Res.* **68**, 1342–1353 (2017).
10. D. P. Crear *et al.*, The impacts of warming and hypoxia on the performance of an obligate ram ventilator. *Conserv. Physiol.* **7**, coz026 (2019).
11. D. K. Cairns, A. J. Gaston, F. Huettmann, Endothermy, ectothermy and the global structure of marine vertebrate communities. *Mar. Ecol. Prog. Ser.* **356**, 239–250 (2008).
12. J. M. Grady *et al.*, Metabolic asymmetry and the global diversity of marine predators. *Science* **363**, eaat4220 (2019).
13. Y. Y. Watanabe, K. J. Goldman, J. E. Caselle, D. D. Chapman, Y. P. Papastamatiou, Comparative analyses of animal-tracking data reveal ecological significance of endothermy in fishes. *Proc. Natl. Acad. Sci. U.S.A.* **112**, 6104–6109 (2015).
14. L. Harding *et al.*, Endothermy makes fishes faster but does not expand their thermal niche. *Funct. Ecol.* **35**, 1951–1959 (2021).
15. J. P. Hayes, T. Garland Jr., The evolution of endothermy: Testing the aerobic capacity model. *Evolution* **49**, 836–847 (1995).
16. L. J. Legendre, D. Davesne, The evolution of mechanisms involved in vertebrate endothermy. *Philos. Trans. R. Soc. B* **375**, 20190136 (2020).
17. C. Sepulveda, N. Wegner, D. Bernal, J. Graham, The red muscle morphology of the thresher sharks (family Alopiidae). *J. Exp. Biol.* **208**, 4255–4261 (2005).
18. B. A. Block, J. R. Finnerty, Endothermy in fishes: A phylogenetic analysis of constraints, predispositions, and selection pressures. *Environ. Biol. Fishes* **40**, 283–302 (1994).
19. J. K. Carlson, K. J. Goldman, C. G. Lowe, Metabolism, energetic demand, and endothermy. *Biol. Sharks Relat.* **10**, 269–286 (2004).
20. C. Pimiento, J. L. Cantalapiedra, K. Shimada, D. J. Field, J. B. Smaers, Evolutionary pathways toward gigantism in sharks and rays. *Evolution* **73**, 588–599 (2019).
21. K. Shimada, The size of the megatooth shark, Otodus megalodon (Lamniformes: Otodontidae), revisited. *Hist. Biol.* **33**, 904–911 (2021).
22. H. G. Ferrón, Regional endothermy as a trigger for gigantism in some extinct macropredatory sharks. *PLoS One* **12**, e0185185 (2017).
23. Y. Kolodny, B. Luz, O. Navon, Oxygen isotope variations in phosphate of biogenic apatites, I. Fish bone apatite–rechecking the rules of the game. *Earth Planet. Sci. Lett.* **64**, 398–404 (1983).
24. J. M. Eiler, "Clumped-isotope" geochemistry–The study of naturally-occurring, multiply-substituted isotopologues. *Earth Planet. Sci. Lett.* **262**, 309–327 (2007).
25. R. A. Eagle *et al.*, Body temperatures of modern and extinct vertebrates from 13C–18O bond abundances in bioapatite. *Proc. Natl. Acad. Sci. U.S.A.* **107**, 10377–10382 (2010).
26. P. Ghosh *et al.*, 13C–18O bonds in carbonate minerals: A new kind of paleothermometer. *Geochim. Cosmochim. Acta* **70**, 1439–1456 (2006).
27. R. A. Eagle *et al.*, Dinosaur body temperatures determined from isotopic (13C–18O) ordering in fossil biominerals. *Science* **333**, 443–445 (2011).
28. R. A. Eagle *et al.*, Isotopic ordering in eggshells reflects body temperatures and suggests differing thermophysiology in two Cretaceous dinosaurs. *Nat. Commun.* **6**, 1–11 (2015).
29. R. R. Dawson *et al.*, Eggshell geochemistry reveals ancestral metabolic thermoregulation in Dinosauria. *Sci. Adv.* **6**, eaax9361 (2020).
30. Y. Miake *et al.*, Ultrastructural studies on crystal growth of enameloid minerals in elasmobranch and teleost fish. *Calcif. Tissue Int.* **48**, 204–217 (1991).
31. P. Iacumin, H. Bocherens, A. Mariotti, A. Longinelli, Oxygen isotope analyses of co-existing carbonate and phosphate in biogenic apatite: A way to monitor diagenetic alteration of bone phosphate? *Earth Planet. Sci. Lett.* **142**, 1–6 (1996).
32. A. Bernard *et al.*, Regulation of body temperature by some Mesozoic marine reptiles. *Science* **328**, 1379–1382 (2010).
33. A. Longinelli, Oxygen isotopes in mammal bone phosphate: A new tool for paleohydrological and paleoclimatological research? *Geochim. Cosmochim. Acta* **48**, 385–390 (1984).
34. B. Ciner, Y. Wang, W. Parker, Oxygen isotopic variations in modern cetacean teeth and bones: Implications for ecological, paleoecological, and paleoclimatic studies. *Sci. Bull.* **61**, 92–104 (2016).
35. J. McCormack *et al.*, Trophic position of Otodus megalodon and great white sharks through time revealed by zinc isotopes. *Nat. Commun.* **13**, 2980 (2022).
36. P. J. Valdes, C. R. Scotese, D. J. Lunt, Deep ocean temperatures through time. *Clim. Past* **17**, 1483–1506 (2021).
37. S. L. Kim *et al.*, Probing the ecology and climate of the Eocene Southern Ocean with sand tiger sharks Striatolamia macrota. *Paleoceanogr. Paleoclimatol.* **35**, e2020PA003997 (2020).
38. S. Zeichner *et al.*, Discrimination factors and incorporation rates for organic matrix in shark teeth based on a captive feeding study. *Physiol. Biochem. Zool.* **90**, 257–272 (2017).
39. A. N. LeGrande, G. A. Schmidt, Global gridded data set of the oxygen isotopic composition in seawater. *Geophys. Res. Lett.* **33**, L12604 (2006).
40. M. Williams *et al.*, Pliocene climate and seasonality in North Atlantic shelf seas. *Philos. Trans. A Math. Phys. Eng. Sci.* **367**, 85–108 (2009).
41. S. J. Jorgensen *et al.*, Eating or meeting? Cluster analysis reveals intricacies of white shark (Carcharodon carcharias) migration and offshore behavior. *PLoS One* **7**, e47819 (2012).
42. E. R. Kast *et al.*, Cenozoic megatooth sharks occupied extremely high trophic positions. *Sci. Adv.* **8**, eabl6529 (2022).
43. S. M. Bernasconi *et al.*, InterCarb: A community effort to improve interlaboratory standardization of the carbonate clumped isotope thermometer using carbonate standards. *Geochem. Geophys. Geosyst.* **22**, e2020GC009588 (2021).
44. S. V. Petersen *et al.*, Effects of improved 17O correction on interlaboratory agreement in clumped isotope calibrations, estimates of mineral-specific offsets, and temperature dependence of acid digestion fractionation. *Geochem. Geophys. Geosyst.* **20**, 3495–3519 (2019).
45. W. F. Defliese, A. Tripati, Analytical effects on clumped isotope thermometry: Comparison of a common sample set analyzed using multiple instruments, types of standards, and standardization windows. *Rapid Commun. Mass Spectrom.* **34**, e8666 (2020).
46. D. Upadhyay *et al.*, Carbonate clumped isotope analysis (Δ47) of 21 carbonate standards determined via gas-source isotope-ratio mass spectrometry on four instrumental configurations using carbonate-based standardization and multiyear data sets. *Rapid Commun. Mass Spectrom.* **35**, e9143 (2021).
47. N. Anderson *et al.*, A unified clumped isotope thermometer calibration (0.5–1,100 C) using carbonate-based standardization. *Geophys. Res. Lett.* **48**, e2020GL092069 (2021).
48. D. York, N. M. Evensen, M. L. Martınez, J. De Basabe Delgado, Unified equations for the slope, intercept, and standard errors of the best straight line. *Am. J. Phys.* **72**, 367–375 (2004).
49. D. Huyghe *et al.*, Clumped isotopes in modern marine bivalves. *Geochim. Cosmochim. Acta* **316**, 41–58 (2022).
50. G. A. Henkes *et al.*, Carbonate clumped isotope compositions of modern marine mollusk and brachiopod shells. *Geochim. Cosmochim. Acta* **106**, 307–325 (2013).
51. N. J. De Winter *et al.*, Absolute seasonal temperature estimates from clumped isotopes in bivalve shells suggest warm and variable greenhouse climate. *Commun. Earth Environ.* **2**, 121 (2021).
52. K. J. Goldman, Regulation of body temperature in the white shark, Carcharodon carcharias. *J. Comp. Physiol. B* **167**, 423–429 (1997).
53. V. A. Tubbesing, B. A. Block, Orbital rete and red muscle vein anatomy indicate a high degree of endothermy in the brain and eye of the salmon shark. *Acta Zool.* **81**, 49–56 (2000).
54. P. C. Sternes, J. J. Wood, K. Shimada, Body forms of extant lamniform sharks (Elasmobranchii: Lamniformes), and comments on the morphology of the extinct megatooth shark, Otodus megalodon, and the evolution of lamniform thermophysiology. *Historical Biol.* **35**, 139–151 (2023).
55. J. A. Cooper *et al.*, The extinct shark Otodus megalodon was a transoceanic superpredator: Inferences from 3D modeling. *Sci. Adv.* **8**, eabm9424 (2022).
56. V. J. Perez, R. M. Leder, T. Badaut, Body length estimation of Neogene macrophagous lamniform sharks (Carcharodon and Otodus) derived from associated fossil dentitions. *Palaeontol. Electron.* **24**, a09 (2021).
57. I. Nakamura, R. Matsumoto, K. Sato, Body temperature stability in the whale shark, the world's largest fish. *J. Exp. Biol.* **223**, jeb210286 (2020).
58. K. Shimada, H. M. Maisch IV, V. J. Perez, M. A. Becker, M. L. Griffiths, Revisiting body size trends and nursery areas of the Neogene megatooth shark, Otodus megalodon (Lamniformes: Otodontidae), reveals Bergmann's rule possibly enhanced its gigantism in cooler waters. *Historical Biol.* **35**, 1–10 (2022).
59. R. W. Boessenecker *et al.*, The Early Pliocene extinction of the mega-toothed shark Otodus megalodon: A view from the eastern North Pacific. *PeerJ* **7**, e6088 (2019).
60. C. Pimiento *et al.*, The Pliocene marine megafauna extinction and its impact on functional diversity. *Nat. Ecol. Evol.* **1**, 1100–1106 (2017).
61. B. K. McNab, Energetics, body size, and the limits to endothermy. *J. Zool.* **199**, 1–29 (1983).
62. T. A. Clarke, Collections and submarine observations of deep benthic fishes and decapod Crustacea in Hawaii. *Pac. Sci.* **26**, 310–317 (1972).
63. T. Vennemann, E. Hegner, G. Cliff, G. Benz, Isotopic composition of recent shark teeth as a proxy for environmental conditions. *Geochim. Cosmochim. Acta* **65**, 1583–1599 (2001).
64. M. Wysokowski, P. Zaslansky, H. Ehrlich, Macrobiomineralogy: Insights and enigmas in giant whale bones and perspectives for bioinspired materials science. *ACS Biomater. Sci. Eng.* **6**, 5357–5367 (2020).
65. B. H. Brattstrom, A. J. Stabile, F. R. Williams, J. Des Lauiers, D. Pope, Body temperature of Indian elephants. *J. Mammal.* **44**, 282–282 (1963).
66. J. C. George, *Growth, Morphology and Energetics of Bowhead Whales (Balaena Mysticetus)* (University of Alaska Fairbanks, 2009).
67. C. M. John, D. Bowen, Community software for challenging isotope analysis: First applications of "Easotope" to clumped isotopes. *Rapid Commun. Mass Spectrom.* **30**, 2285–2300 (2016).
68. A. Mine *et al.*, Microprecipitation and δ18O analysis of phosphate for paleoclimate and biogeochemistry research. *Chem. Geol.* **460**, 1–14 (2017).
69. C. Lécuyer, R. Amiot, A. Touzeau, J. Trotter, Calibration of the phosphate δ18O thermometer with carbonate–water oxygen isotope fractionation equations. *Chem. Geol.* **347**, 217–226 (2013).
70. M. L. Griffiths *et al.*, Clumped isotope data for bioapatite temperature calibration and assessment of Otodus megalodon body temperature, Version 1.0. Interdisciplinary Earth Data Alliance (IEDA). https://doi.org/10.26022/IEDA/112933. Deposited 12 June 2023.